East African Journal of Biophysical and Computational Sciences

Journal homepage : https://journals.hu.edu.et/hu-journals/index.php/eajbcs

The Effect of CuO Nanoparticle Variation on the Green Synthesized ZnO/CuO Nanocomposites for Antibacterial Activities

Bulti Abdisa Kerayu[1], Hundessa Alemu[1], Gemechis Fikadu[1], Asefa Keneni[2], Tibebu Alemu[1,3*]

[1]*Department of Chemistry, College of Natural and Computational Sciences, Ambo University, Ambo, Ethiopia*

[2]*Department of Biology, College of Natural and Computational Sciences, Ambo University, Ambo, Ethiopia*

[3]*School of Graduate Studies, Ambo University, Ambo, Ethiopia*

KEYWORDS:

Orange peel extract;

ZnO/CuO nanocomposites;

Antibacterial activity;

Surface characterization;

Green synthesis;

UV-Vis spectroscopy

Research article

ABSTRACT

Plant extracts play critical role in synthesizing nanomaterials for a wide range of applications in human health and managing environmental pollutions. The present work focuses on varying CuO NP's concentration in ZnO/CuO nanocomposites (NC) synthesized with orange peel extracts (ZnO/CuO WE NC) for its antibacterial activities. The concentration of CuO with respect to ZnO NP fixed in 10:10, 10:20, 10:30, and 10:40. The as-synthesized NC is characterized using UV-Vis, FTIR, XRD, and SEM spectroscopes. Accordingly, the UV-Vis result reveals that the absorption spectra range from 312-328 nm confirming the incorporation of extract to provide strong absorption peaks along with the increasing concentration of CuO in the nanocomposite while it energy band gap of ZnO/CuO WE NC was narrowed from 3.97 to 3.78 eV. FTIR analysis revealed that the stretching vibration of Zn-O and Cu-O are observed around 480 cm^{-1} and 600 cm^{-1}, respectively in all ratios of WE NC. XRD indicated that the formation of hexagonal wurtzite structure and the crystallite size recorded in 24.12 to 3.17 nm. The SEM image showed the morphology of 10:20, 10:30, and 10:40 are aggregated, smooth, polished, and smaller size compared to 10:10 ZnO/CuO WE NC. The antibacterial activities of 10:10, 10:20, 10:30, and 10:40 ZnO/CuO WE NC were remarkable especially, 10:40 ZnO/CuO WE NC provided strong activity against *P. aeruginosa*. Thus, the as-synthesized 10:40 ZnO/CuO WE NC is so profound to combat bacterial infectious diseases.

INTRODUCTION

Nanotechnology is a rapidly evolving science field focused on the design, synthesis, and manipulation of materials (nanomaterials) at the nanometric scale (1–100 nm) with wide-ranging applications (Singh *et al*., 2015). Among nanomaterials, metal oxide nanoparticles (NPs) have garnered significant attention because of their unique phyisicochemical properties, including high surface area, chemical stability, and antimicrobial efficacy (Mihindukulasuriya and Lim, 2014; Benelmekki, 2015; Khan *et al*., 2019; Kumari *et al*., 2023). The growing

*Corresponding author:
Email: tibebu.alemu@ambou.edu.et, +251909117127 https://dx.doi.org/10.4314/eajbcs.v6i1.4S

challenge of antibiotic resistance necessitates an alternative antimicrobial strategies, and metal oxide NPs have emerged as promising candidates due to its stability and broad-spectrum activity (Sawai, 2003; Shi *et al*., 2014). For example, zinc oxide (ZnO) and copper oxide (CuO) NPs exhibited antibacterial effects through multiple mechanisms, including reactive oxygen species (ROS) generation, membrane disruption, and ion release leading to bacterial cell death (Mantecca *et al*., 2015). ZnO, an n-type semiconductor with a wide band gap (3.37 eV), offers excellent stability and biocompatibility, making it suitable for biomedical and environmental applications (Sirelkhatim *et al*., 2015; Bekru *et al*., 2022). In contrast, CuO, a p-type semiconductor with a narrow band gap, demonstrates strong antibacterial and antifungal properties due to its ability to generate ROS (Yulizar *et al*., 2018; Naseem and Durrani, 2021). The integration of ZnO and CuO in to nanocomposites (NCs) enhances charge separation, reduces electron-hole recombination, and improves visible-light absorption, thereby augmenting their antibacterial effectiveness (Bekru *et al*., 2022).

Scholars have developed various synthesization techniques of NPs, among which green methods have emerged as a promising approach that leverages plant-derived biomolecules. These synthesis methods offer several advantages over conventional or widely accepted approaches, including sustainability, reduced toxicity and controlled particle morphology (Abid *et al*., 2022; Kumar *et al*., 2023). Example, ZnO NPs synthesized using orange peel extract effectively inhibited *E. coli* and *S. aureus* under ambient conditions (Thi *et al*., 2020). In similar case, ZnO/CuO NCs have been prepared using *Zingiber officinale* extract demonstrated strong antibacterial effect against both gram positive and gram negative bacterial (Takele *et al*., 2023). In addition, Gao *et al*., (2020) reported that biogenic ZnO NPs enhanced the shelf-life of fresh strawberries, highlighting their potential in food preservation (Luque *et al*., 2018; Gao *et al*., 2020). Recently, Alemu *et al*. (2023) developed ZnO/CuO NCs in orange peel extract and recorded outstanding inhibition of gram-positive bacteria growth. Although the aforementioned and other studies demonstrated exceptional antibacterial performance upon CuO NPs incorporation, the optimal concentration for maximum antibacterial effect or efficacy was not clearly determined yet. Therefore, a systematic investigation into the effect of CuO NPs concentration in the NCs on bacterial growth inhibition remains unexamined. This research aims to address the gap observed through optimizing the CuO NP content in ZnO/CuO NCs synthesized using orange peel extract and concomitantly assessed their antibacterial effectiveness against selected bacterial strains. The findings will contribute to the growing field of green nanotechnology by providing scientific insights into the synthesis, optimization, and antibacterial applications of ZnO/CuO NCs, thereby promoting sustainable and effective antimicrobial solutions.

MATERIALS AND METHODS

Materials

Zinc nitrate hexahydrate ($Zn(NO_3)_2.6H_2O$, purity: 99%, India), Zinc acetate dihydrate ($Zn(CH_3COO)_2.2H_2O$, purity: 98%, India), Copper (II) nitrate trihydrate ($Cu(NO_3)_2.3H_2O$, UNI-CHEM Chemical Reagents, purity: 99%, India), sodium hydroxide (NaOH, Ran chem

Industry and Trading, purity: 99.5%, Germany), Absolute Ethanol (CH_3CH_2OH, Purity: 99.99%, India) analytical grades were used for this study. *Pseudomonas aeruginosa* (Gram-negative) and *Staphylococcus aureus* (Gram-positive) bacteria were Isolated, cultured and tested in biology laboratory, Ambo University, Ethiopia.

Preparation of Orange peel extract

Orange peels were collected from the market of Ambo town, Oromia region, Ethiopia. After thoroughly washing and rinsing with deionized (DI) water, the fruit was peeled, air dried for 12 hours and about 4 kg taken which was ready for extraction process. The dried peel was then ground into a moderately fine powder. Afterward, 1 gm of the powder was placed in different glass containers with 50 mL of DI water in each container and was stirred for 3 hrs. Once macerated, each mixture was placed in a water bath for 60 min at 60 ºC. Finally, the mixture was filtered, and the resulting extract was stored (Figure 1) in a refrigerator of 4 ºC (Manokari *et al*., 2016).

Figure 1: Orange fruits peel purchased from Ambo market for extraction process

Synthesization of ZnO/CuO nanocomposite (NC) with Orange Peel extract (WE)

The ZnO/CuO NC in orange peel extract (ZnO/CuO WE) was prepared via mixing 2 g of each Zn $(NO_3)_2.6H_2O$ and Zn $(CH_3COO)_2.2H_2O$ dissolved separately in 42.5 mL of orange peel extracts. This mixture was then continuously stirred for 60 min once placed in a water bath at 60 ºC. Subsequently, the mixture was dried at 150 ºC and then heated for 1 hr at 400 ºC. The organic substances in orange peel extract supposed to act as ligating agents as shown in Alemu *et al*., (2023). The hydroxyl aromatic ring groups in the extract could form complex molecules with Zn^{2+} and Cu^{2+} ions. Through, the process of nucleation and shaping followed by calcination at 400 ˚C, it was resulted in the formation of ZnO/CuO NC (Çolak and Karaköse, 2016). The concentration of ZnO/CuO WE varied from 10:10, 10:20, 10:30 and 10:40 ppm in the ratio of ZnO:CuO NP via changing the concentration of only CuO NP to study its effect on the antibacterial activity (Singh *et al*., 2018).

Reaction mechanism in the synthetization of ZnO/CuO WE NC

Figure 2 display the possible reaction mechanism during the synthesis process of ZnO/CuO NC using orange peel extract (ligation process takes place between the functional groups of the orange peel and the respective precursors). The phytochemicals components in orange peel extracts could act as ligand agents and forms complex compounds between OH group of the organic molecules and Zn^{2+} and Cu^{2+} ions. The corresponding nanoparticles are formed and stabilized through a nucleation process, while the mixture of organic components decomposes upon calcination, reducing the ions and resulting in the formation of ZnO/CuO nanocomposites (Thi *et al*., 2020). Lastly, Zn^0 and Cu^0 gets oxidized to mixture of ZnO/CuO NC upon calcination (Ahmed *et al*., 2022) while the presence of organic components are used as capping agent

to prevent the NPs agglomerations (Veisi *et al*., 2021).

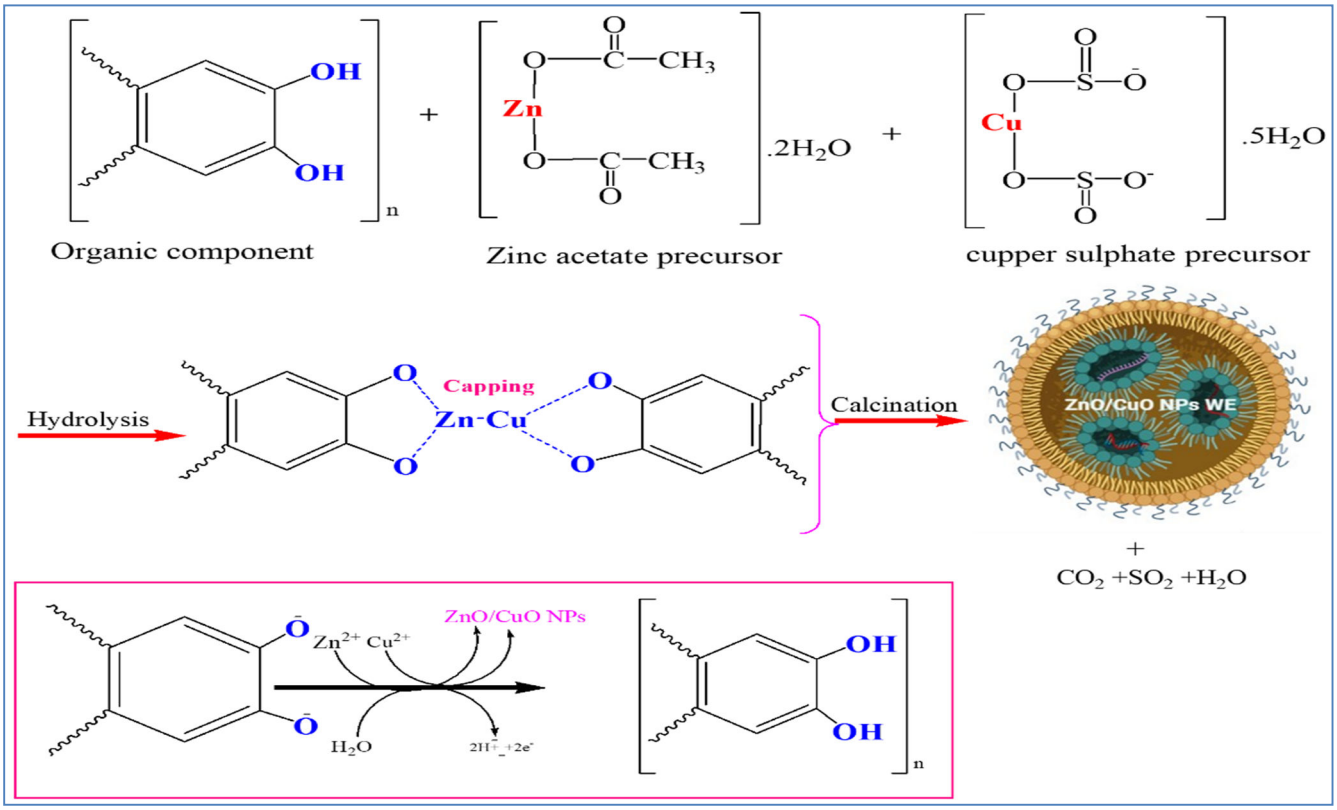

Figure 2: Proposed mechanism for the formation of functionalized ZnO/CuO WE NC.

Characterization of ZnO/CuO WE NC

The surface characterizations of ZnO/CuO WE NC were studied using X-ray diffraction (XRD) (SHIMADZU Corporation (Japan), XRD-7000 X-RAY DIFFRACTOMETER) for crystalline structure study. Fourier transform infrared (FTIR) (IS 50 ABX, Germany) was used to reveal functional group of NC. Whereas, UV-Vis spectrophotometer (OPTIZEN TOP, KOREA) was used to investigate the chemical properties and its energy band gap while the morphology of ZnO/CuO WE NC was characterized by scanning electron microscope (SEM) (EVO18, CARL ZEISS).

Antibacterial Activities

The antibacterial activities of the synthesized ZnO/CuO WE were done using two human pathogenic bacteria strains i.e., *Staphylococcus aureus* (Gram-positive) and *Pseudomonas aeruginosa* (Gram-negative). The agar well diffusion method was used for the evaluation of the antibacterial activity of as-synthesized ZnO/CuO WE NC. Muller Hinton (MH) Agar plates were prepared, sterilized, and solidified. After solidification, 10^6 colony forming units (CFU) of bacterial cultures were swamped on solidified MH Agar plates. Five wells were cut out in the agar layer of the plate using an aluminum bore of 2 mm diameter for the

synthesized ZnO/CuO WE NC (Perez-Gavilan *et al*., 2021) with different concentration (10:10, 10:20, 10:30, and 10:40 for ZnO:CuO). Then, 50 µl of each of the synthesized NC, positive control (Cloxacillin), and negative control (DMSO) was dropped into the wells using a micropipette and then incubated at 37 ˚C for 18 hrs. At the end of the incubation period, the antibacterial activities of the synthesized NC were checked by observing and measuring the zone of inhibition.

RESULTS AND DISCUSSION

Characterization of Nanocomposite

UV-Vis spectroscopic analysis: The UV-Vis spectra of the 10:10, 10:20, 10:30, and 10:40 ZnO/CuO WE NC is shown in Figure 3. The absorption peaks of the as-synthesized NC were found at the interval of 320-334 nm which fall under visible region and its sharp absorption feature indicates that each ratio of ZnO:CuO NC is monodispersed in nature. The UV-Vis spectra signify that the strong absorption peaks (Figure 3(a)) has formed in the visible region, which ascribed the presence of biomolecules from the orange peel extract (Dey *et al*., 2021). These characteristic absorbance peaks for each ZnO:CuO ratio indicate the successful formation of NCs with adsorbed biomolecules. The results indicate that the synthesized ZnO:CuO WE NCs achieved optimal reduction for tested ratio whereas 10:20 ZnO:CuO WE NC exhibited highest absorbance at longer wavelength comparing to the remaining components. This spectral shift is attributed to the formation of smaller particle sizes comparing to 10:10, 10:30 and 10:40 ZnO:CuO WE NCs as a result of the quantum confinement effect (Matinise *et al*., 2017). In addition, the 10:20 ZnO:CuO WE NC possesses the lowest energy band gap (Table 1) suggesting enhanced electron mobility.

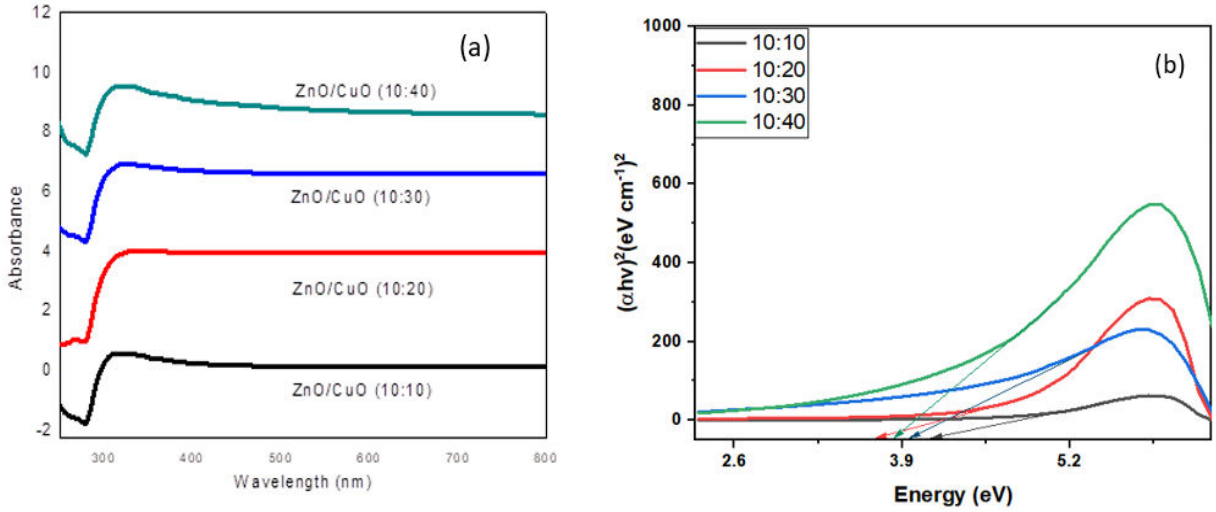

Figure 3: UV-Vis spectra (a), Tauc plot for the energy bandgap determination for ZnO/CuO (10:10, 10:20, 10:30 and 10:40).

The band gap energy of the synthesized NPs was determined using equation (Eq. 1) below.

$$E_g = {}^{hc}/_{\lambda} \quad (1)$$

Where, h = Planck's constant (6.63 x 10^{-34} m^2 kg s^{-1}), c = speed of light (3.00 x 10^8 ms^{-1}), λ = Absorption wavelength in UV region (330 nm).

The energy band gap values for the synthesized ZnO/CuO WE NCs, as presented in Table 1, were calculated to be 3.97 eV, 3.78 eV, 3.85 eV, and 3.83 eV for the 10:10, 10:20, 10:30, and 10:40 ratios, respectively. These results indicate that as the ZnO:CuO ratio changes from 10:10 to 10:20, the band gap energy decreases (Eq. 1), suggesting that the 10:20 ZnO/CuO WE NC exhibits the most effective visible light absorption. This finding aligns with the results obtained from the Tauc plot. Furthermore, the experimental results are consistent with theoretical values, which typically range from 3.02 to 1.47 eV. However, the observed band gap values are slightly higher than those reported by Qamar *et al*. (2017). The UV-Vis absorption spectrum of the synthesized NPs shows absorption at lower wavelengths (312–328 nm) for all NCs. Therefore, UV-Vis spectroscopy characterization further confirms the successful formation of ZnO/CuO WE NCs in the expected absorption range.

Table 1: The energy band gap calculated from UV-vis data for ZnO/CuO WE NC.

Ration of ZnO/CuO WE NC	Wavelength (λ_{max}) in nm	The energy band gap (E_{bg}) in eV
10:10	312	3.97
10:20	328	3.78
10:30	322	3.85
10:40	324	3.83

FT-IR Spectroscopic Analysis: FT-IR spectra of the prepared ZnO/CuO WE NC were recorded to determine its functional groups in the range of 4000–400 cm^{-1} (Figure 4). According to the results, the spectra of all ratios in ZnO/CuO WE NC demonstrated the absorption band exhibited at 3200-3500 cm^{-1} represents the stretching vibrations of –OH group of adsorbed H_2O molecule on the surface of NCs (Nuisin *et al*., 2022). On the other hand, the stretching vibrations observed at 1105, 1391, 1590 and 1606 cm^{-1} show C-O stretching, C-H bending, C=O and C=C bonds (Berra *et al*., 2018), respectively in all combination. In addition, the intense absorption peaks observed at 609, 715, and 973 cm^{-1} correspond to the stretching vibrations of Zn–O, Cu–O, and Zn–O–Cu bonds within the nanocomposites (Li *et al*., 2022). The intensity of these peaks increased with the rise in CuO concentration, while the nature of the functional groups remained unchanged, confirming that the composition of the nanocomposites remained consistent across different CuO concentrations.

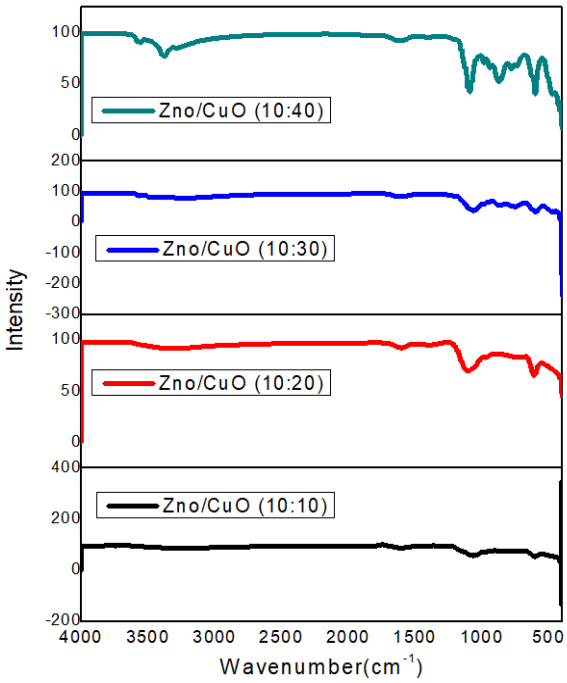

Figure 4: FTIR spectra of synthesized ZnO/CuO WE NC.

X-Ray Diffraction (XRD) Analysis: The XRD patterns of ZnO/CuO WE NCs are shown in Figure 5, covering the 2θ range of 10–80°. The diffraction peaks for ZnO/CuO WE NCs with different concentrations were observed at 2θ = 35.90°, 36.76°, 42.40°, and 42.51°, corresponding to the lattice planes (002), (101), (012), and (012), respectively. These peaks confirm the hexagonal crystalline phase of the ZnO/CuO WE NCs, agreed with the JCPDS card No. 36-1451. Additionally, a slight shift in the 2θ positions of certain peaks was observed. This shift may be attributed to variations in CuO concentration during the preparation of the samples using orange peel extract, which could influence the crystallographic structure of the NCs. The average crystalline size of ZnO/CuO-WE NCs for each ratio is calculated using Debye-Scherrer's equation.

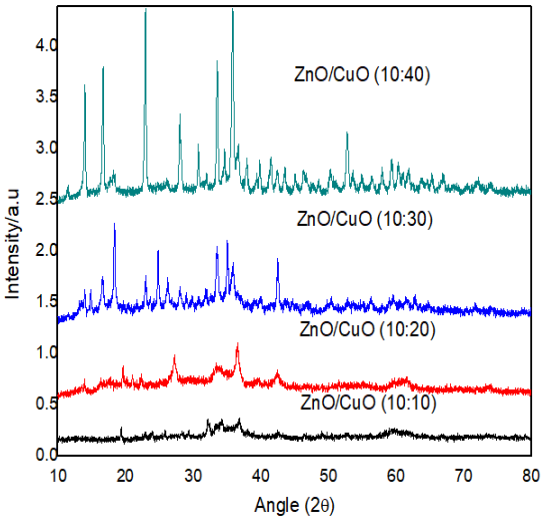

Figure 5: XRD patterns of the as-synthesized ZnO/CuO WE NC.

Accordingly, the average crystalline size (D_p) of 10:10, 10:20, 10:30 and 10:40 ZnO/CuO WE NC were 24.12, 16.33, 6.64 and 3.17 nm (Table 2). The result confirmed that the size of the NCs has decreased as the increasing concentration of CuO within the composites. In the current study, the presence of different functional groups including C–O, C=O, and O–H in the plant extract contribute to stabilizing particles while an increase amount of CuO increase the crystal growth of ZnO/CuO WE NC.

Table 2: Crystalline size determination for ZnO/CuO-WE nanocomposites.

Nanocomposite	2θ	θ	cosθ	FWMH	in rad	size/nm	Aver/nm
CuO/ZnO (10:10)	32.3	16.15	0.96053	0.3548	0.00603	23.95119	24.12
	34.1	17.05	0.95604	0.3705	0.00629	23.04399	
	36.71	18.355	0.94909	0.3392	0.00576	25.35469	
CuO/ZnO (10:20)	27.46	13.73	0.97142	0.54702	0.00929	15.36071	16.33
	36.71	18.355	0.94909	0.52469	0.00892	16.39122	
	42.44	21.22	0.93219	0.50779	0.00863	17.24380	
CuO/ZnO (10:30)	18.58	9.29	0.98688	1.4827	0.02521	6.713731	6.64
	24.69	12.345	0.97685	1.2446	0.02116	6.713731	
	35.20	17.6	0.95319	1.3191	0.02242	6.491789	
CuO/ZnO (10:40)	22.97	11.485	0.9799	2.6707	0.04541	3.118995	3.17
	33.46	16.73	0.95767	2.6707	0.04541	3.191395	
	35.95	17.975	0.95119	2.6707	0.04541	3.213137	

Analysis of Surface Morphology: The morphology of 10:10, 10:20, 10:30, and 10:40 for ZnO/CuO WE NC was studied using SEM (Figure 6). The SEM image of 10:10 ZnO/CuO WE NC indicates that the crystal formed has cluster and flake-like structure while the particles are agglomerated in nature.

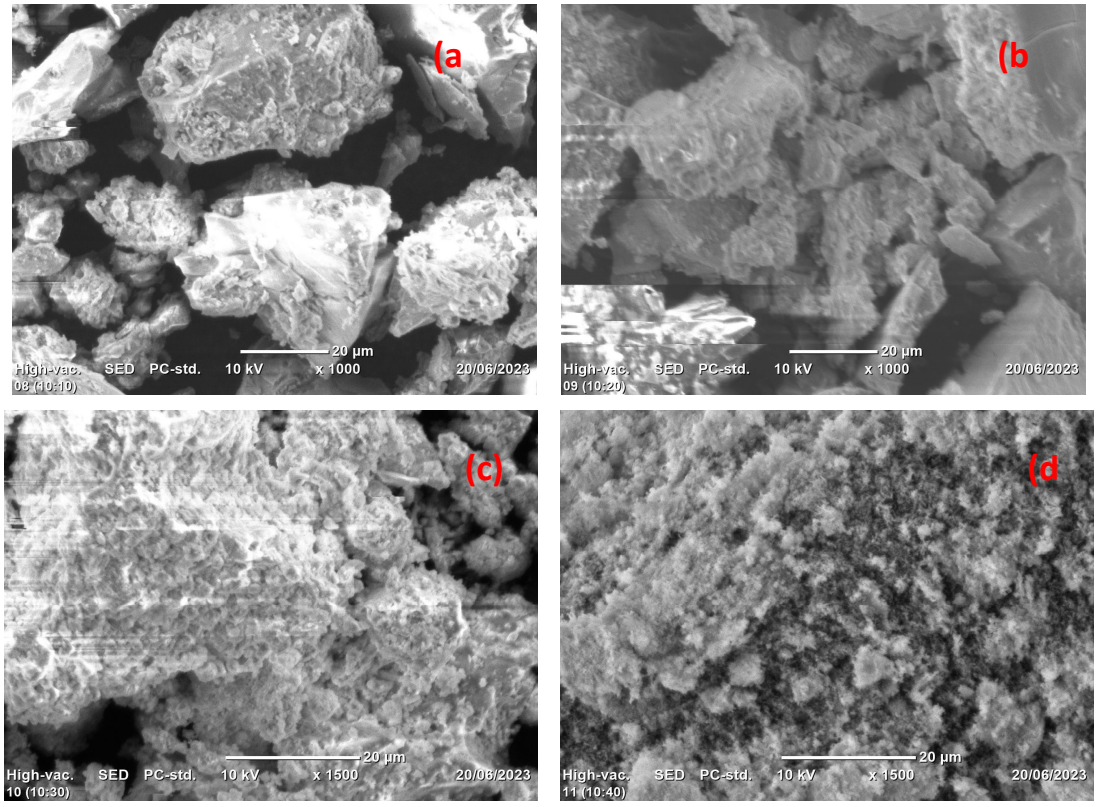

Figure 6: SEM images of ZnO/CuO WE NC (a) 10:10, (b) 10:20, (c) 10:30, and (d) 10:40 in ZnO:CuO ratio.

The images of the 10:20 and 10:30 ZnO/CuO WE NCs exhibit aggregated, smooth, and polished surfaces with smaller particle sizes compared to 10:10 ZnO/CuO WE NC. Notably, the 10:40 ZnO/CuO WE NC displays a finer distribution of smaller particles with a porous-like structure. These findings confirm that the grain size and overall morphology of the synthesized NCs are strongly influenced by the CuO NP concentration under identical reaction conditions. Furthermore, the crystal sizes of 10:10, 10:20, 10:30, and 10:40 ZnO/CuO WE NCs increased, as determined using the Scherrer equation. The images clearly reveal microstructural heterogeneities and distinct morphological differences among the synthesized NCs, highlighting the effect of CuO content on their structural properties.

Study of Antibacterial Activity

For each synthesized nanomaterial, the zone of inhibition (ZOI) values was recorded as shown in Table 3. The antibacterial effect of nanomaterials against both bacteria compared with control samples, the diameter of ZOI varied at the different concentration levels of NCs. The three trials of antibacterial activities of 10:10, 10:20, 10:30, 10:40 ZnO/CuO WE NC were measured and showed a good response against *S. aureus* with an average maximum ZOI of 17.33, 21.66, 25.33 and 28.66 mm while its activity against *P. aeruginosa* was shown relatively higher ZOI of 21.00, 25.66, 28.33 and 30.66 mm after 18 hrs incubation times. This indicates that 10:10, 10:20, 10:30, and 10:40 ZnO/CuO WE NC in particular 10:40 ZnO/CuO WE NC are more effective for *P. aeruginosa* than *S. aureus* bacterial strain.

Table 3: Antibacterial activity of NC applied to two human pathogenic bacteria.

Nanocomposites	Test organism	Zone of inhibition (mm)				
		Trial-1	Trial-2	Trial-3	Average	Cloxacillin
10:10 ZnO/CuO WE NC	*S. aureus*	14	13	25	17.33	35
	P. aeroginosa	22	27	14	21.00	35
10:20 ZnO/CuO WE NC	*S. aurous*	19	22	24	21.66	35
	P. aeroginosa	27	20	30	25.66	35
10:30 ZnO/CuO WE NC	*S. aurous*	25	26	25	25.33	35
	P. aeroginosa	30	30	25	28.33	35
10:40 ZnO/CuO WE NC	*S. aurous*	29	30	27	28.66	35
	P. aeroginosa	30	35	27	30.66	35

This suggests that Gram-negative bacteria exhibited higher susceptibility to the synthesized 10:40 ZnO/CuO WE NC, as their loosely structured cell membranes provide less protection against external attacks. Figure 7 and 8 confirm the formation of larger inhibition zones for bacterial strains, represented as 1 (10:10), 2 (10:20), 3 (10:30), and 4 (10:40) ZnO/CuO WE NC, against Gram-positive and Gram-negative bacteria, respectively. The highest concentration (sample 4) demonstrated the most effective zone of inhibition (ZOI) compared to the others. Therefore, the antibacterial effectiveness of the nanomaterials increases with the CuO NP concentration in the

ZnO/CuO WE NC synthesized using orange peel extracts (Wang *et al*., 2017).

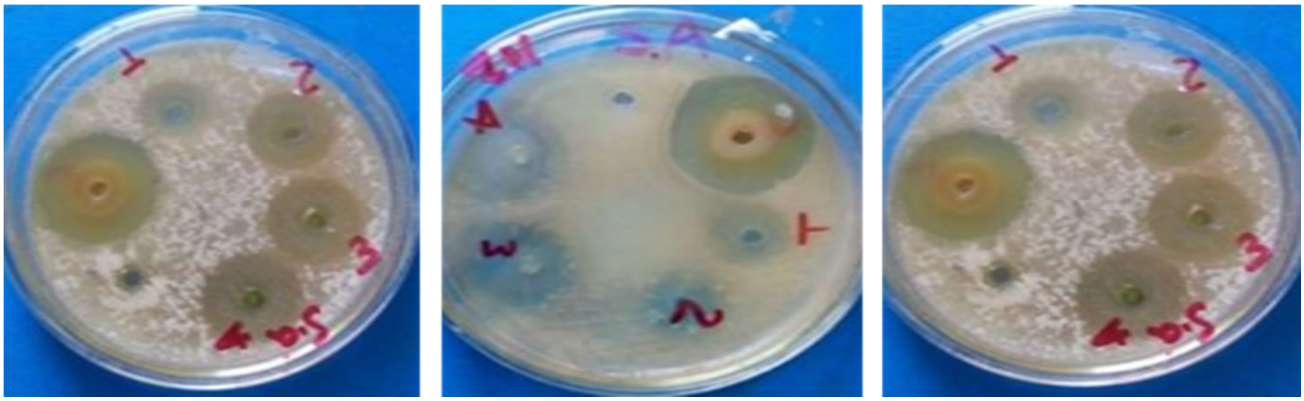

Figure 7: The antibacterial activity of ZnO/CuO WE NC against *S. aureus* bacteria.

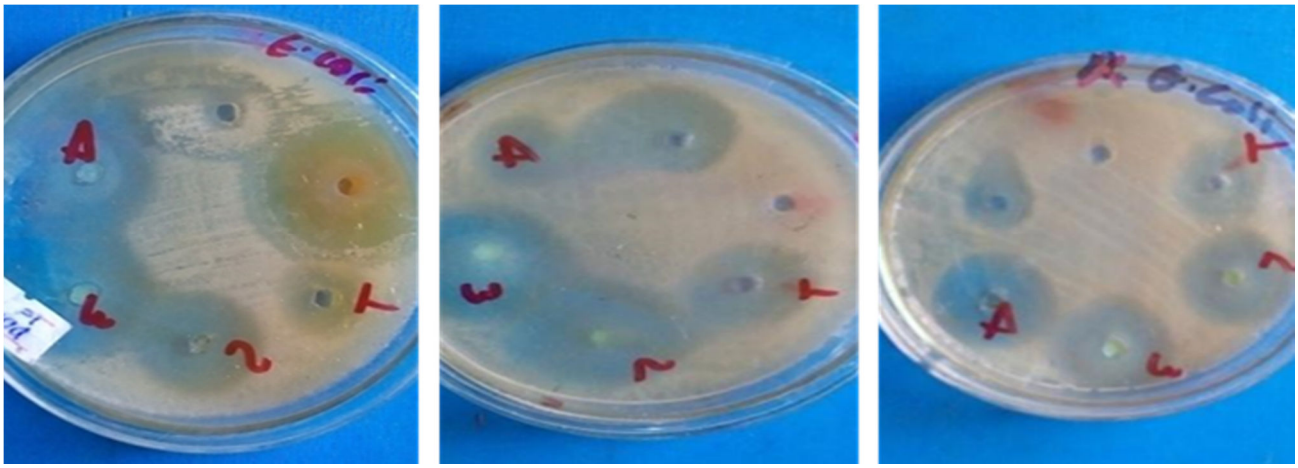

Figure 8: The antibacterial activity of ZnO/CuO WE NC against *P. aeroginosa* bacteria

The results of this study indicated that the antibacterial activities of 10:10, 10:20, 10:30, and 10:40 ZnO/CuO WE NC is CuO NP concentration dependent. The negative control (DMSO) did not show any ZOI whereas the positive control (Cloxacillin) showed the highest ZOI. Based on the results of the current study, it was evident that the ZOI of samples (Figure 7 and 8) showed that the synthesized compounds significantly inhibited the selected bacterial probably by generating ROS species that can easily penetrate the bacterial wall particularly when the ratio of ZnO to CuO WE changed from 10:10 to 10:40. The ROS generated by NC provides better contact environment with bacteria (Khan *et al*., 2016; Kumar *et al*., 2017). Therefore, this study provides valuable insights into overcoming bacterial resistance to standard antibiotic drugs and offers a potential solution to serious health-related issues. The synthesized nanocomposite (NC) could serve as a viable alternative to antibiotic-resistant drugs due to its cost-effectiveness, non-toxic nature, and sustainable production from renewable and environmentally

friendly materials (Chinemerem Nwobodo *et al*., 2022).

CONCLUSION

In this work, we have studied the effect of CuO NP concentration variation of ZnO/CuO NC prepared with orange peel extract for the study of antibacterial activities. The as-synthesized materials were characterized by SEM, XRD, FTIR, and UV-VIS for the investigation of its morphology, crystal structure, functional group, and energy band gap. The XRD study confirms the formation of hexagonal wurtzite structure and the crystallite size of 24.12 - 3.17 nm, the vibrational stretching band was found around 480-600 cm^{-1} reveal that the WE NC possesses the metal-oxygen bonds, and SEM image signify that each ratio of ZnO/CuO WE NC affects the grain size and anti-bacterial activity of ZnO/CuO WE NC. The characteristic absorption peak observed at 312-328 nm also supports the formation of 10:10, 10:20, 10:30, and 10:40 of ZnO/CuO WE NC with a very narrow energy gap with 3.97-3.78 eV. Among all WE NC with various ZnO:CuO NC ratio, 10:40 ZnO/CuO WE NC exhibited better antibacterial activity against both human pathogens particularly to *P. aeroginosa* bacteria.

Declaration of interest

The authors declare no conflict of interest.

Acknowledgements

The author would like to forward heartfelt gratitude to Ambo University for providing the essential facilities and support that contributed to the successful completion of this research.

References

Abid N., Khan A. M., Shujait S., Chaudhary K., Ikram M., Imran M., Maqbool M. 2022. Synthesis of nanomaterials using various top-down and bottom-up approaches, influencing factors, advantages, and disadvantages: A review. *Adv. Colloid Interface Sci.* 300: 102597.

Ahmed A. A., Rizvi Z. R., Shahzad H. and Farrukh M. A. 2022. Neodymium oxide nanoparticles synthesis using phytochemicals of leaf extracts of different plants as reducing and capping agents: Growth mechanism, optical, structural and catalytic properties. *J. Chin. Chem. Soc.* **69**(3): 462-475.

Alemu T., Asefa G., Shumbura M., Kenani A. and Tullu A. M. 2023. Biosynthesization of ZnO/CuO Nanocomposites in Orange Peel Crude Extract for Antibacterial Activities. *J. Sci. Sustain. Dev.* **11**(2): 94-110.

Bekru A. G., Tufa L. T., Zelekew O. A., Goddati M., Lee J. and Sabir F. K. 2022. Green Synthesis of a CuO–ZnO Nanocomposite for Efficient Photodegradation of Methylene Blue and Reduction of 4-Nitrophenol. *ACS Omega* **7**(35): 30908-30919.

Benelmekki M. 2015. An introduction to nanoparticles and nanotechnology. In: Benelmekki M. (Ed.) *Designing Hybrid Nanoparticles*. Morgan & Claypool Publishers. doi: 10.1088/978-1-6270-5469-0ch1

Berra D., Salah Eddine L., Boubaker B., Mohammed Ridha O., Berrani D. and Achour R. 2018. Green synthesis of copper oxide nanoparticles by Pheonix dactylifera l leaves extract. *Digest J. Nanomater. Biostruct.* **13**: 1231-1238.

Chandra H., Kumari P., Bontempi E. and Yadav S. 2020. Medicinal plants: Treasure trove for green synthesis of metallic nanoparticles and their biomedical applications. *Biocatal. Agric. Biotechnol.* **24**: 101518.

Nwobodo D. C, Ugwu M. C., Anie C.O, Al-Ouqaili M. T. S., Ikem J. C, Chigozie U. V. and Saki M. 2022. Antibiotic resistance: The challenges and some emerging strategies for tackling a global menace. *J. Clin. Lab. Anal.* **36**(9): e24655.

Çolak H. and Karaköse E. 2016. Green synthesis and characterization of nanostructured ZnO thin films using Citrus aurantifolia (lemon) peel extract by

spin-coating method. *J. Alloys. Compd.* **690**: 658-662.

Dey S., Basha S. R., Babu G. V. and Nagendra T. 2021. Characteristic and biosorption capacities of orange peels biosorbents for removal of ammonia and nitrate from contaminated water. *Cleaner Materials*, 1: 100001. ISSN 2772-3976.

Doan Thi T. U., Nguyen T. T., Thi Y. D., Ta Thi K. H., Phan B. T. and Pham K. N. 2020. Green synthesis of ZnO nanoparticles using orange fruit peel extract for antibacterial activities. *RSC Advances* **10**(40): 23899-23907.

Gao Y., Xu D., Ren D., Zeng K. and Wu X. 2020. Green synthesis of zinc oxide nanoparticles using Citrus sinensis peel extract and application to strawberry preservation: A comparison study. *LWT* **126**: 109297. doi: 10.1016/j.lwt.2020.109297

Joudeh N. and Linke D. 2022. Nanoparticle classification, physicochemical properties, characterization, and applications: a comprehensive review for biologists. *J. Nanobiotechnol.* **20**(1): 262. doi: 10.1186/s12951-022-01477-8

Khan I., Saeed K. and Khan I. 2019. Nanoparticles: Properties, applications and toxicities. Arabian *J. Chem.* **12**(7): 908-931.

Khan S. T., Musarrat J. and Al-Khedhairy A. A. 2016. Countering drug resistance, infectious diseases, and sepsis using metal and metal oxides nanoparticles: Current status. *Colloids Surf B Biointerfaces*. **146**: 70-83.

Kumar A., Shah S. R., Jayeoye T. J., Kumar A., Parihar A., Prajapati B. and Kapoor D. U. 2023. Biogenic metallic nanoparticles: biomedical, analytical, food preservation, and applications in other consumable products. *Front. Nanotechnol.* **5**. doi: 10.3389/fnano.2023.1175149.

Kumar R., Umar A., Kumar G. and Nalwa, H. S. 2017. Antimicrobial properties of ZnO nanomaterials: A review. *Ceram. Int.* **43**(5): 3940-3961.

Kumari N., Sudharsan V., Muthu Kutty T., Jayan N. and Laxmi Deepak Bhatlu M. 2023. Green synthesis and characterization of Zinc and Copper oxides nanocomposite using Phyllanthus emblica extracts and its antibacterial and antioxidant properties. *Materials Today: Proceedings*. doi: https://doi.org/10.1016/j.matpr.2023.06.287

Li M., Chen Z., Yang L., Li J., Xu J., Chen C. and Liu T. 2022. Antibacterial Activity and Mechanism of GO/Cu2O/ZnO Coating on Ultrafine Glass Fiber. *Nanomater.* **12**(11): 1857.

Luque P., Soto-Robles C. A., Nava O., Gómez C., Castro-Beltrán A., et al. 2018. Green synthesis of zinc oxide nanoparticles using Citrus sinensis extract. *J. Mater. Sci.: Mater. Electron*. **29**. doi: 10.1007/s10854-018-9015-2

Manokari M, Ravindran C.P. and Shekhawat M. S 2016. Biosynthesis of Zinc oxide Nanoparticles using Melia azedarach L. extracts and their Characterization. *Int. J. Pharm. Sci. Res.* **1**:31-36.

Mantecca P., Moschini E., Bonfanti P., Fascio U., Perelshtein I., Lipovsky A., et al. 2015. Toxicity Evaluation of a New Zn-Doped CuO Nanocomposite With Highly Effective Antibacterial Properties. *Toxicol Sci*. **146**(1): 16-30.

Matinise N., Fuku X. G., Kaviyarasu K., Mayedwa N. and Maaza M. 2017. ZnO nanoparticles via Moringa oleifera green synthesis: Physical properties and mechanism of formation. *Appl. Surf. Sci.* **406**: 339-347.

Mihindukulasuriya S. D. F. and Lim L. T. 2014. Nanotechnology development in food packaging: A review. *Trends Food Sci. Technol.* **40**(2) 149-167.

Mohammadi-Aloucheh R., Habibi-Yangjeh A., Bayrami A., Latifi-Navid S. and Asadi A. 2018. Enhanced anti-bacterial activities of ZnO nanoparticles and ZnO/CuO nanocomposites synthesized using Vaccinium arctostaphylos L. fruit extract. *Artif Cells Nanomed Biotechnol.* **46**(sup1): 1200-1209.

Müller K., Bugnicourt E., Latorre M., Jorda M., Echegoyen Sanz Y., Lagaron J. M. et al. 2017. Review on the Processing and Properties of Polymer Nanocomposites and Nanocoatings and Their Applications in the Packaging, Automotive and Solar Energy Fields. *Nanomater*. (Basel) **7**(4). 74. doi: 10.3390/nano7040074

Nadaroglu H., Güngör A. A. and Selvi, İ. 2017. Synthesis of nanoparticles by green synthesis method. *Int. J. Innov. Res. Rev.* **1**(1): 6-9.

Naseem T. and Durrani T. 2021. The role of some important metal oxide nanoparticles for wastewater and antibacterial applications: A review. *J. Environ. Chem. Ecotoxicol.* **3**: 59-75.

Nuisin R., Siripongpreda T., Watcharamul S., Siralertmukul K. and Kiatkamjornwong S. 2022. Facile Syntheses of Physically Crosslinked Carboxymethyl Cellulose Hydrogels and Nanocomposite Hydrogels for Enhancing Water Absorbency and Adsorption of Sappan Wood Dye. *ChemistrySelect* **7**(10), e202104598. doi: https://doi.org/10.1002/slct.202104598

Palmero P. 2015. Structural Ceramic Nanocomposites: A Review of Properties and Powders' Synthesis Methods. *Nanomater.* (Basel) **5**(2): 656-696. doi: 10.3390/nano5020656

Perez-Gavilan A., de Castro J. V., Arana A., Merino S., Retolaza A., Alves S. A., et al. 2021. Antibacterial activity testing methods for hydrophobic patterned surfaces. *Sci. Rep.* **11**(1): 6675. doi: 10.1038/s41598-021-85995-9

Qamar M. T., Aslam M., Rehan Z. A., Soomro M. T., Basahi, J. M., Ismail, I. M. I., et al. 2017. The

influence of p-type Mn3O4 nanostructures on the photocatalytic activity of ZnO for the removal of bromo and chlorophenol in natural sunlight exposure. *Appl. Catal. B: Environ*. **201**: 105-118.

Sani e Z., Iqbal M. S., Abbas K. and Qadir M. I. 2022. Synthesis, characterization and evaluation of biological properties of selenium nanoparticles from Solanum lycopersicum. *Arab. J. Chem.* **15**(7): 103901. doi: https://doi.org/10.1016/j.arabjc.2022.103901

Sawai J. 2003. Quantitative evaluation of antibacterial activities of metallic oxide powders (ZnO, MgO and CaO) by conductimetric assay. *J. Microbiol. Methods* **54**(2): 177-182. doi: 10.1016/s0167-7012(03)00037-x

Shi L. E., Li Z. H., Zheng W., Zhao Y. F., Jin Y. F. and Tang Z. X. 2014. Synthesis, antibacterial activity, antibacterial mechanism and food applications of ZnO nanoparticles: a review. *Food Addit. Contam. Part A Chem. Anal. Control Expo. Risk Assess.* **31**(2): 173-186.

Singh A., Singh N. B., Hussain I., Singh H. and Singh S. 2015. Plant-nanoparticle interaction: An approach to improve agricultural practices and plant productivity. *Int. J. Pharm. Sci. Invent.* **4**: 2319-6718.

Singh J., Dutta T., Kim K.-H., Rawat M., Samddar P. and Kumar P. 2018. 'Green' synthesis of metals and their oxide nanoparticles: applications for environmental remediation. *J. Nanobiotechnol*. **16**(1): 84. doi: 10.1186/s12951-018-0408-4

Sirelkhatim A., Mahmud S., Seeni A., Kaus N. H. M., Ann L. C., Bakhori, S. K. M., et al. 2015. Review on Zinc Oxide Nanoparticles: Antibacterial Activity and Toxicity Mechanism. *Nano-micro. Lett*. **7**(3): 219-242. doi: 10.1007/s40820-015-0040-x

Stoimenov P., Klinger R., Marchin G. and Klabunde K. 2002. Metal Oxide Nanoparticles as Bactericidal Agents. *Langmuir* **18** (17): 6679-6686. doi: 10.1021/la0202374

Takele E., Feyisa Bogale R., Shumi G. and Kenasa G. 2023. Green Synthesis, Characterization, and Antibacterial Activity of CuO/ZnO Nanocomposite Using Using Zingiber officinale Rhizome Extract. J. Chem. 3481389. doi: 10.1155/2023/3481389

Thi T. U. D., Nguyen T. T., Thi Y. D., Thi K. H. T., Phan B. T. and Pham K. N. 2020. Green synthesis of ZnO nanoparticles using orange fruit peel extract for antibacterial activities. *RSC Advances* **10**(40): 23899-23907.

Veisi H., Karmakar B., Tamoradi T., Hemmati S., Hekmati M. and Hamelian M. 2021. Biosynthesis of CuO nanoparticles using aqueous extract of herbal tea (Stachys Lavandulifolia) flowers and evaluation of its catalytic activity. *Sci. Rep*. **11**(1): 1-13.

Wang L., Hu C. and Shao L. 2017. The antimicrobial activity of nanoparticles: present situation and prospects for the future. *Int. J. Nanomedicine*. **12**: 1227-1249. doi: 10.2147/ijn.S121956

Yulizar Y., Bakri R., Apriandanu D. O. B. and Hidayat T. 2018. ZnO/CuO nanocomposite prepared in one-pot green synthesis using seed bark extract of Theobroma cacao. Nano-Struct. Nano-Objects **16**: 300-305.